SYNTHESIS OF SILICA-POLY(ETHYLENE GLYCOL)-POLY(HEXYL METHACRYLATE): NOVEL NANOPARTICLE-ORGANIC HYBRID MOLECULES

A Thesis

Presented to the Faculty of the Graduate School

of Cornell University

in Partial Fulfillment of the Requirements for the Degree of

Masters of Science

by

Laura Lynne Olenick

August 2009

ABSTRACT

Organic-inorganic hybrid molecules are of increasing interest due to the ability to increase the dispersion of the inorganic component in a system which would ordinarily lead to aggregation.[1-3] A well-dispersed and well-understood system is important in industry for ease of manufacturing as well as for customer satisfaction.[4] In *The Structure and Rheology of Complex Fluids,* Larson uses the example of toothpaste. Unless the components of the toothpaste are evenly dispersed with even texture, consumers will not purchase the product.

The goal of this research is to synthesize, characterize and study the properties of organic-inorganic hybrid molecules. These novel nanoparticle-organic hybrid molecules, or NOHMS, were synthesized using silica, a triethoxysilane-terminated poly(ethylene glycol), and poly(hexyl methacrylate) polymerized using atom transfer radical polymerization (ATRP) of hexyl methacrylate.[5-6]

Scheme 1. A Schematic Diagram for the Preparation of SiO_2-PEG-PHMA Nanoparticle-Organic Hybrid Molecules (NOHMS).

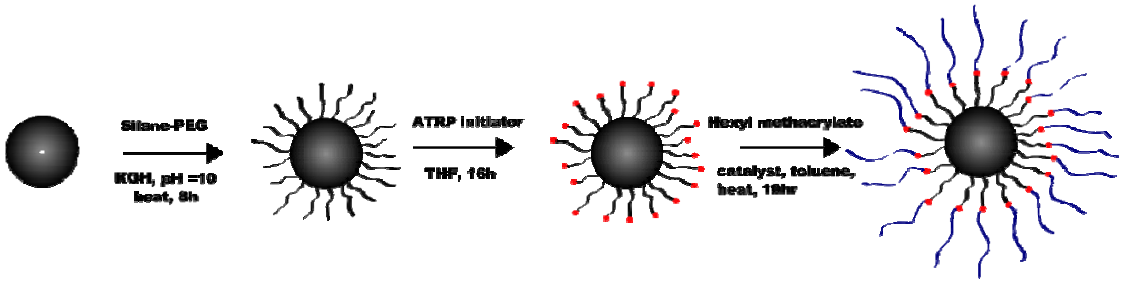

Six samples are discussed here of varying molecular weights of poly(hexyl methacrylate) (PHMA). These six samples targeted degrees of polymerization of

PHMA of 5, 7, 9, 11, 15, and 20. Each sample contained approximately the same amount of poly(ethylene glycol) (PEG). Three samples of poly(ethylene glycol) monomethyl ether-*b*-poly(hexyl methacrylate) (MPEG-PHMA) are also discussed here for comparison purposes. Thermogravimetric analysis (TGA) shows a percentage of weight remaining after heating to 550^{o}C indicating presence of inorganic material in the hybrid samples. TGA of the free samples show 100% weight loss by 400^{o}C. Differential scanning calorimetry (DSC) of the hybrid samples showed one glass transition temperature (T_g), a melting point, and a crystallization point for each sample. The T_g was found not to correspond to the T_g of PEG or of PHMA. The crystallization point was found to depend on volume fraction of the silica. Dynamic light scattering (DLS) measurements show a single, though broad, peak with an average radius of around 30 nm. FT-IR shows peaks in the NOHMS consistent with SiO_2-PEG-PHMA. Using rheology, the hybrid molecules were found to have yield stresses that are dependent upon the volume fraction of the silica core. The rheology of the free block copolymers did not show a yield stress for any of the samples.

BIOGRAPHICAL SKETCH

Laura Lynne Olenick was born in Wheeling, W.V. on September 3, 1982. She grew up in Manalapan, NJ with her parents and brother. Laura studied chemistry at Colby College in Waterville, ME. During her time there, she researched the structure and function of small inorganic molecules under the guidance of Professor Rebecca Conry. She graduated from Colby College in 2004 with a Bachelor of Arts in Chemistry. Before beginning graduate school at Cornell, Laura spent time living and working in Boulder, CO while enjoying the Rocky Mountains. Though the mountains were breathtakingly beautiful, she could not resist the urge to return to the lab. In September of 2007, she began her studies in Chemical Engineering at Cornell University in Ithaca, NY.

to Renea Malinky, Joseph Olenick, Thomas Olenick and Brenton Cox,

without them this would not be possible.

ACKNOWLEDGMENTS

I would like to thank my advisor, Professor Lynden Archer, for his guidance and advice throughout this project, for his patience and dedication to his students, for believing in my abilities, for pushing me farther than I thought I could go, and for his infectious enthusiasm for science. I would also like to thank my committee member Professor Claude Cohen for his advice and support and for allowing the use of equipment in his lab.

I would also like to extend my gratitude to Audrey Cohen, an undergraduate student who worked with me on this research project during the summer of 2008.

I also thank the members of Dr. Archer's research group, including: Praveen Agarwal, Lucas Landherr, Dr. Zhenyu Quian, Haibo Qi, Keesha Hayes, Zichao Yang, and Alexandra Corona. Their challenging questions, engaging arguments and sincere curiosity have made this research better and this experience an enjoyable and memorable one.

TABLE OF CONTENTS

LIST OF TABLES

LIST OF SCHEMES

LIST OF FIGURES

INTRODUCTION

Nanoparticle–polymer nanocomposites are of current interest due to novel properties stemming from the benefits of combining inorganic and organic components – the rigidity and thermal stability of the inorganic material and the flexibility and ductility of the organic component.[7] In this paper, the inorganic component is the core and the organic component is the covalently bonded polymer. This type of nanocomposite has the advantage of well-dispersed SiO_2 in a polymer that will not settle or aggregate over time. The ability for the nanoparticles to remain within the polymer over time implies applications in coatings[8], sensors[9], photoresist materials[10], and a wide variety of other industrial uses. Metal oxides in some catalysts have been used to remove CO, NO_x and SO_x from the atmosphere.[11] One interesting use could be in oil excavation owing to the ability to tune the viscosity of this material and the functionality of this material via the choice of polymer and the molecular weight of that polymer and also owing to the low vapor pressure of these materials.

These nanocomposites, as a new group of hybrid molecules, offer variety in chemical nature – both in the inorganic and organic components, in shape – nanoparticles can take several geometric shapes, such as spheres, cubes, or rods, and in dispersion state – the size and density of the nanoparticles coupled with the stabilization forces from the polymer, which can be either van der Waals, hydrogen bonding, or electrostatic, will affect its dispersion state.[12] Using a nanoparticle with an enormous surface area per unit volume to tether a functional polymer, greatly inceases the functionality per molecule ratio compared to the untethered polymer.[12]

In addition to the choice of polymer and molecular weight, these nanocomposites also offer options in how to attach the polymer to the inorganic core. One approach is the “attach to” approach whereby a polymer of a controlled molecular

weight is synthesized, one end of the polymer is functionalized and then reacted with the core.[9, 13] In this approach, sterics play an important role in the graft density of the polymer on the core. A polymer with a high molecular weight may only be able to attach to a few places on the core before sterics block any further reactions. The main benefit to this approach is the ability to synthesize the polymer to a low polydispersity index (PDI). Another benefit is strong control over the molecular weight of the polymer.

The competing approach is the "grow from" approach.[1, 14-20] In this approach, the inorganic core is first reacted with a small molecule initiator. This initiator is able to bond to the core with a higher graft density than a functionalized polymer. The core-initiator molecule is then used as an initiator for controlled living polymerization (CLP).

In this paper, the CLP process utilized is atom transfer radical polymerization (ATRP). The benefit of using ATRP is that the conditions are not as stringent as for anionic or cationic polymerization,[14, 21] but still allows molecular weight,[22] polydispersity,[23] polymer composition[24] and polymer architecture to be well controlled.[2, 25] The less stringent conditions allow for an easier, more straightforward synthesis. Another benefit of using ATRP over other living radical polymerizations is that the use of the catalyst prevents bimolecular termination events.[26] The catalyst insures that following the addition of each monomer to the propagating species, that the propagating species is "capped" with the halogen atom which has been transferred from the catalyst. This capping, which is reversible[27], guarantees that the propagating radical species will not interact with each other, terminating the reaction. This reversible activation, deactivation of the propagating species allows for more control over molecular weights and molecular weight dispersities than previously favored

radical polymerizations which were centered on irreversible redox processes.[18] (It should be noted here also, that the tacticity of the polymers synthesized using ATRP is almost the same as the tacticity of the polymers created using conventional radical initiators and was not affected by sterically large or chiral ligands.[28])

ATRP is also growing in popularity because it can be used for a wide variety of monomers – methacrylates, acrylates, styrenes, acrylonitrile, dienes, acrylamides, methylacrylamides.[1, 18, 25, 27] The catalyst system, which includes a halogenated metal coupled with a ligand, can be tailored to fit these monomers. In choosing the appropriate catalytic system, it is important to take into account monomer and polymer solubility,[27] halogenated metal solubility,[27] the redox potential of the catalyst system,[29-31] and the activity of the carbon-halogen bond in the initiator and monomer.[18] For a catalyst system to be effective, the lower oxidation state of the metal center should be more stable than the higher oxidation state so that there exists a low concentration of the radical species.[18] The initiator should be chosen to complement the catalyst system.[32-33] Also, polymerization rates and molecular weight dispersities can be improved by additives[34-35] and this should be taken into account if the needed catalytic system for the chosen monomer does not produce the desired result. The additive, $Al(Oi\text{-}Pr)_3$, for example, was shown by Ando et al. to stabilize the higher oxidation state of the metal complex to aid in the radical generation from the dormant species.[34]

MATERIALS AND METHODS

Unless otherwise stated, all materials were purchased from Sigma-Aldrich.

Synthesis of PEO covered silica nanoparticles

[Hydroxy(polyethylyeneoxy)propyl]triethoxysilane, 50% in ethanol (SIH6188.0, silane-PEO, PEO MW between 500 and 550) was used as received from Gelest, Inc. Water, potassium hydroxide (KOH), and silicon dioxide nanoparticles (Ludox SM-30, 30% in water) were used as received from Sigma-Aldrich.

Ludox solution was diluted to 5 % (w/v). In a 500mL media bottle, water was added to the silane-PEO solution to dilute the solution to 25% (w/v). A 20% KOH/water solution was added to the diluted silane-PEO solution until a pH of 10 was reached. The diluted Ludox solution was added dropwise while stirring to the silane-PEO solution to prevent aggregation of the silicon dioxide nanoparticles. This Ludox-silane-PEO solution was placed, uncapped in a 100^{o}C oil bath for 1 hour. The solution was ultrasonicated for 15 minutes and returned to the 100^{o}C oil bath for 1 hour. The solution was ultrasonicated for another 15 minutes and returned to the oil bath for 6 hours. The ultrasonication was done to prevent aggregation of the nanoparticles and promote even graft density of the silane-PEO to the nanoparticles.

In order to remove free silane-PEO this solution was dialyzed in water for 2 days using snake-skin dialysis tubing of 10MWCO from ThermoFisher Scientific. The dialyzed solution was put in a large petri dish and placed in a convection oven, uncovered, at 70^{o}C until all of the water had evaporated.

The nanoparticle-silane-PEO was collected from the petri dish and stored in a 100 mL media bottle in a glovebox under argon.

Synthesis of initiator coated nanoparticles

Scheme 2. Preparation of SiO_2-PEG-2bb Nanoparticle-Organic Hybrid Molecules (NOHMS).

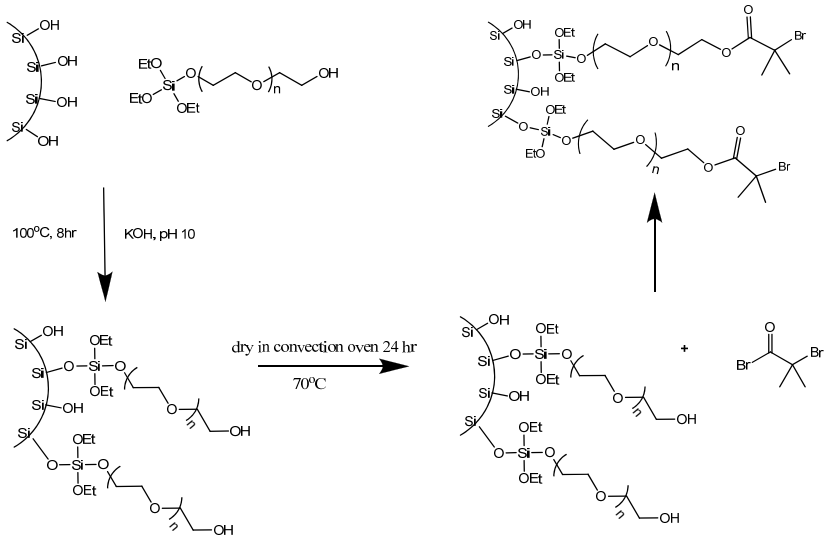

Tetrahydrofuran (THF) was purified in a solvent still under nitrogen using 1,1-diphenylethylene 97% and *n*-butyllithium. 1,1-diphenylethylene was added in a ratio of 1 drop to 50mL THF. *n*-butyllithium was added in a ratio of 1mL to 50mL THF. After approximately 2 days, the purified THF was vacuum distilled and stored under argon.

2-bromoisobutyrl bromide (2-b-b) was vacuum distilled under nitrogen and stored in a glovebox under argon prior to use.

Triethylamine (Et_3N) was purified using approximately 10 wt % of calcium hydride. This solution was stirred uncapped for 24 hours and then capped and kept stirred at room temperature until used. Prior to use, Et_3N was vacuum distilled under nitrogen and stored in a glovebox under argon.

For the following calculation, it is necessary to determine the graft density of the silane-PEO on the nanoparticle-PEO molecule. The graft density is found through thermogravimetric analysis (TGA). Regardless of whether or not the amount of silane-peo determined from the TGA is bonded or free, the silane-peo will react with 2-b-b. Therefore, in determining the amount of 2-b-b to add to the nanoparticle-PEO sample, the mass used is the loss seen from the TGA.

Synthesis of Poly(hexyl methacrylate)-grafted nanoparticles (PHMA-*g*-SiO_2)

Scheme 3. Preparation of SiO_2-PEG-PHMA Nanoparticle-Organic Hybrid Molecules (NOHMS).

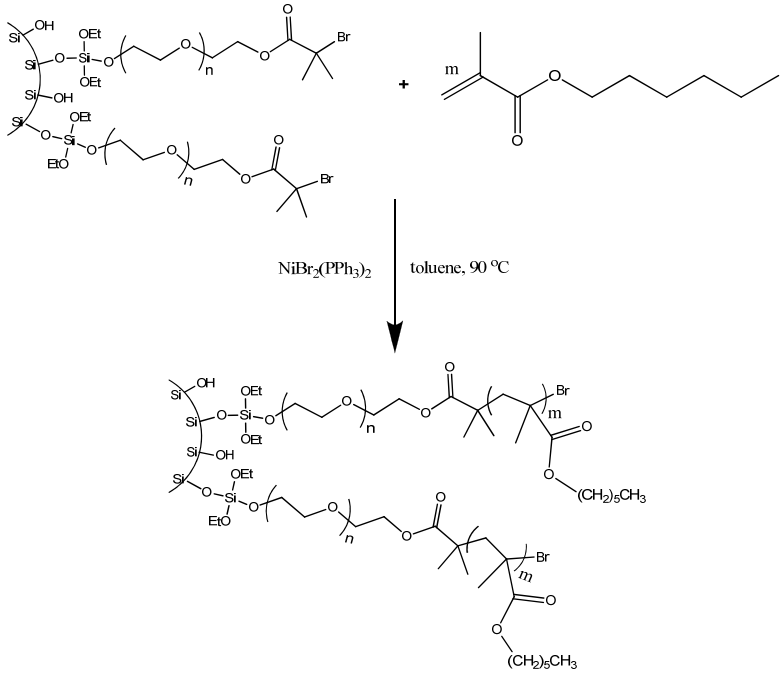

The ATRP of PHMA followed the procedure described in Mahajan et al.[5-6]

Toluene was purified with approximately 10 wt. % calcium hydride. This solution was stirred for 24 hours and then capped, covered with parafilm and stored at room

temperature. Immediately prior to use, toluene was distilled and placed in the glovebox under argon. Hexyl methacrylate was stirred over CaH_2 overnight then vacuum distilled and placed into a glovebox.

In a glovebox, under Argon, the functionalized SiO_2-peo-2bb solution was added to a round bottom flask. To this flask purified toluene, nickel catalyst and hexyl methacrylate were added. The flask was capped with a rubber septum and placed in a 90^{o}C oil bath in a glovebox under nitrogen. Nitrogen was continually flowed through the glovebox and a large 16 gauge needle was placed through the rubber septum. The needle allowed THF gas release, since the boiling point of THF is below 90^{o}C. This reaction was allowed to continue for 10 hours. After 10 hours, the reaction was taken out of the glovebox, exposed to oxygen to stop the catalyst and placed in the refrigerator to prevent further polymerization.

The nickel catalyst was removed through a column of neutral alumina and distilled until a small amount of solvent remained. (For more information about this purification process please see Appendix A.)The solution was dialyzed in chloroform for 3 rounds of solvent changes totaling approximately 24 hours. After dialysis, the solution was placed in a 100 mL media bottle and put in a vacuum oven at 80^{o}C. The resulting NOHMS were stored capped at room temperature.

HF etching of SiO_2

Approximately 300 mg of NOHMS were mixed with $NH_4 \cdot$ HF and stirred for 24 hours at room temperature, following a procedure similar to that in Mandal et al.[36] The polymer was then extracted from the solution via separation with toluene. The toluene layer was washed with distilled water 4 times and then removed with rotary evaporation. Figure 1 illustrates the results of the HF etching of the SiO_2 cores.

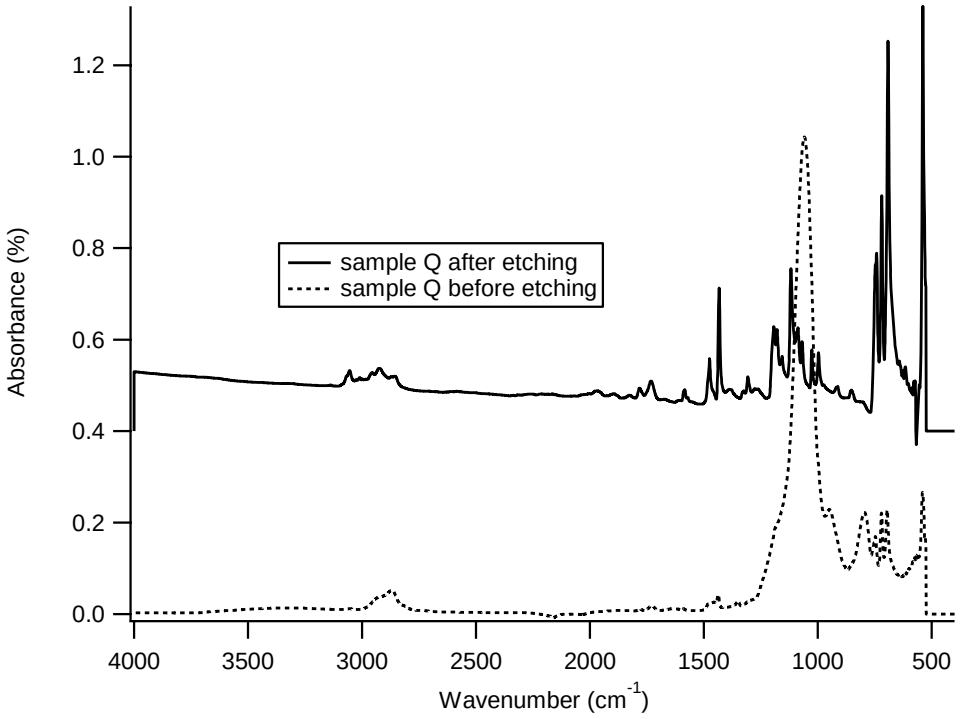

Figure 1. FT-IR spectrum of Absorbance v. Wavenumber for SiO2-PEG-PHMA (sample Q) before and after etching of the SiO_2 cores with HF.

RESULTS AND DISCUSSION

NMR

^{1}H NMR experiments on PEG-2bb were carried out on a ARX Bruker 300MHz NMR in deuterated chloroform with trimethylsiloxane as a reference.

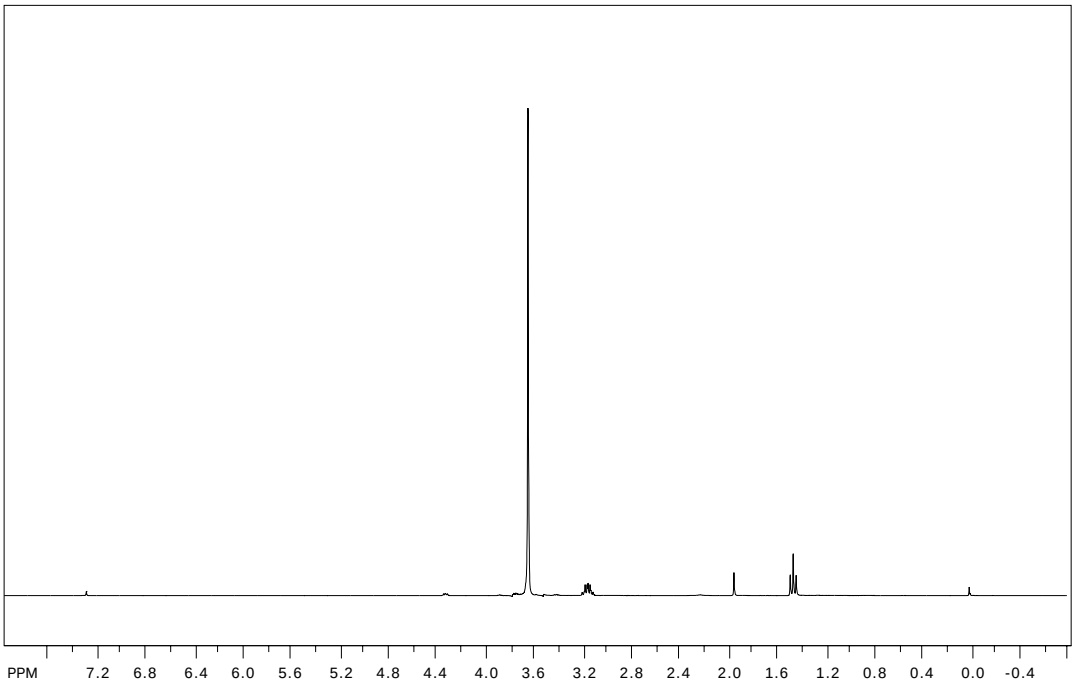

Figure 2. ^{1}H NMR spectrum of PEG-2bb.

The spectrum shown in Figure 2 is consistent with the spectra of Mahajan et al.[5] with the exception of the small quintet around 3.18 ppm. This quintet has been difficult to identify. Using the capability of the software program, ChemDraw, several molecules potentially responsible for this peak have been eliminated as candidates for this peak. From ChemDraw, triethylamine shows a triplet at 1.01 ppm and a quartet at 3.02 ppm. PEG shows a very strong peak near 4.0 ppm, but no peaks between 3.5 and 0 ppm. 2-bromoisobutyrl bromide shows peaks near 1.2 ppm. However, due to the

consistency with Mahajan et al. it is likely that this spectrum shows the presence of PEG-2bb and a small amount of contaminant. It is this author's recommendation that this experiment be duplicated and this NMR repeated to determine whether this is contamination and not a by-product of the reaction.

Thermogravimetric Analysis and Differential Scanning Calorimetry

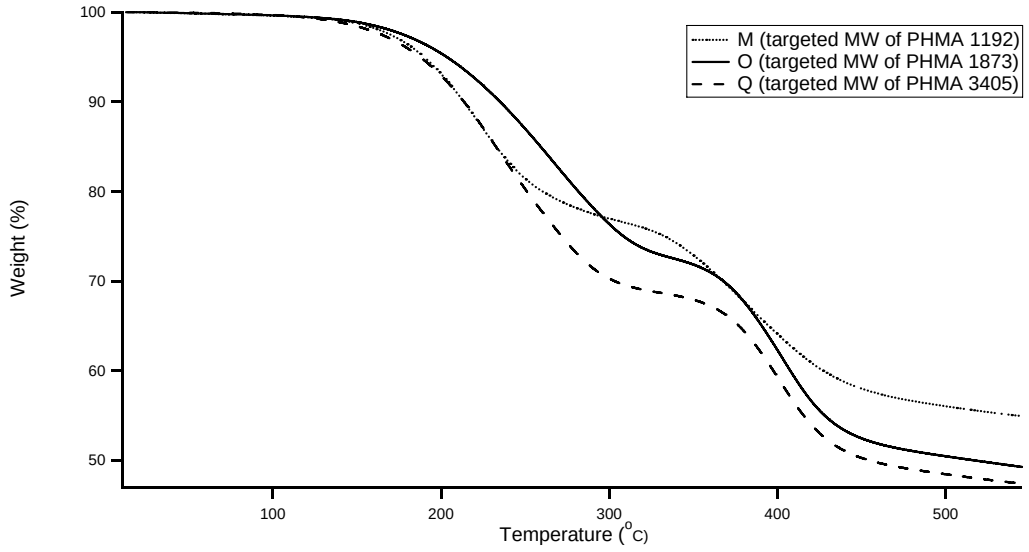

Figure 3. Percent Weight v. Temperature for SiO_2-PEG-PHMA samples of varying targeted molecular weights of PHMA. Samples were purified using dialysis in chloroform for a period of 3 days and dried in vacuo prior to testing. Samples were heated at a rate of 10°C /min under atmosphere of nitrogen.

Thermogravimetric analysis (TGA) was carried out from room temperature to 550°C using a TA Instruments Q500 under an atmosphere of nitrogen at heating rate

of 10°C/min. Figure 3 shows the percentage of weight remaining in the sample as a function of temperature. The large amount of weight remaining after heating to 550 °C indicates presence of inorganic material.

Notable in Figure 3 is the presence of two distinct plateau regions. These inflection points are made even more apparent when the derivative of the data is taken. These derivative plots are shown in Figure 4. These two regions of large weight loss is likely due to an initial burning of polymer forming a charred layer that must be burned through before the next layer of polymer can burn. These two regions are not present in the TGA graphs of MPEG-550, PEG-1450, or PEG-300 as shown in Figure 5. These two regions are also not present in SiO_2 as shown in Figure 6. These two regions do show in the PEG-PHMA samples (samples X, Y and Z), Figure 7.

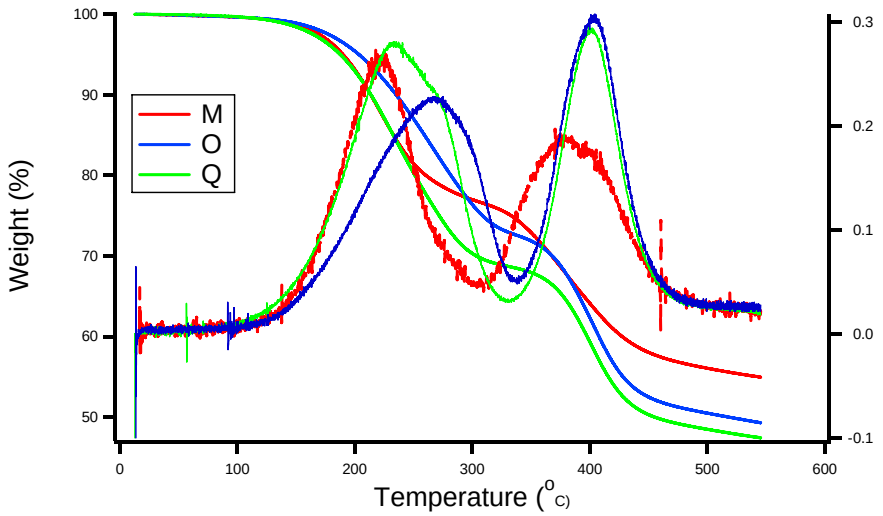

Figure 4. Percent Weight v. Temperature for SiO_2-PEG-PHMA samples M, O, and Q as well as the derivative of each of those graphs. See Figure 2 for details on the TGA conditions.

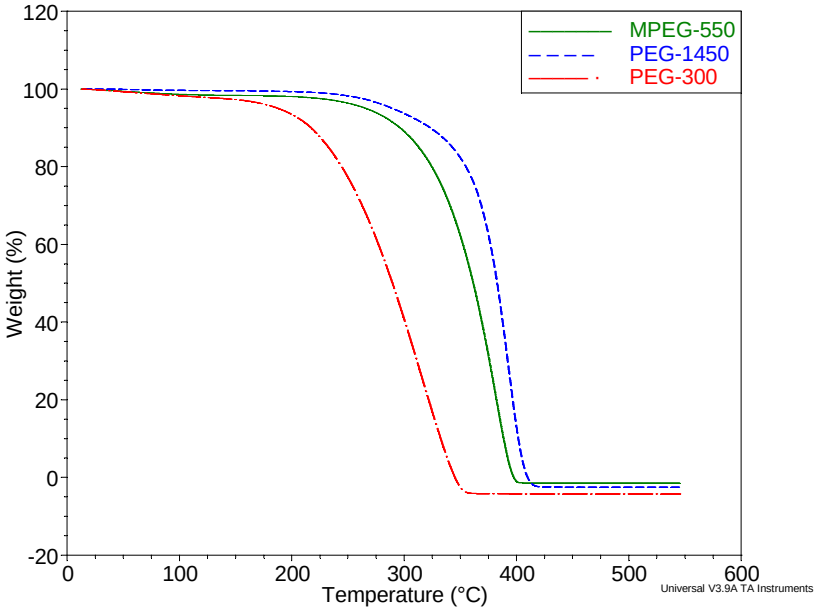

Figure 5. Percent Weight v. Temperature for MPEG-550, PEG-1450, and PEG-300. See Figure 2 for details on the TGA conditions.

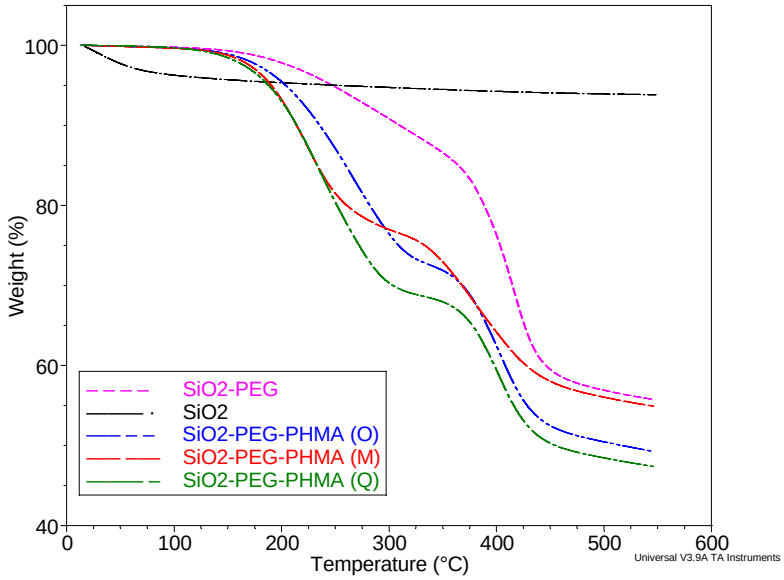

Figure 6. TGA curves for SiO_2, SiO_2-PEG, SiO_2-PEG-PHMA (samples M, O, and Q). See Figure 2 for details on TGA conditions.

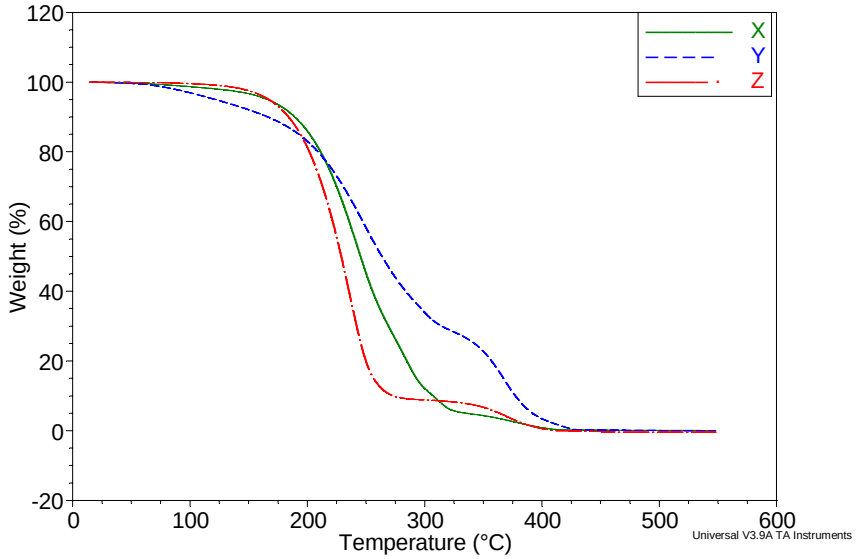

Figure 7. TGA curves for PEG-PHMA (samples X, Y and Z).

Table 1 uses the data from the TGA to estimate the volume fraction of SiO_2 in each sample according to the following equation:

$$Estimated\ Volume\ Fraction\ of\ SiO_2 = \frac{mass\ (SiO_2)/\rho(SiO_2)}{mass\ (SiO_2)/\rho(SiO_2)\ +\ mass\ (PHMA-\mathrm{b}-PEG)/\rho(PHMA-\mathrm{b}-PEG)}$$

where ρ is the mass density of the component following in parentheses. The values used are as follows: ρ(SiO_2) = 2.2 g/cm^3,[37] mass(SiO_2) and mass(PHMA-*b*-PEG) were read from the TGA results, and ρ(PHMA-*b*-PEG) was estimated to be the density of PHMA.[38] This author recommends that a more extensive study be done to determine the density of PHMA-*b*-PEG at room temperature for varying molecular weights of PHMA. This study would yield the needed results for a more accurate calculation of the volume fraction of SiO_2 in each of the samples.

Table 1. Estimated Volume Fraction of SiO_2 in six samples of SiO_2-PEG-PHMA

Sample Name	Targeted MW of PHMA	% Weight at 545°C	Estimated Volume Fraction of SiO2
L	851	52.8326	0.338932205
M	1192	54.9347	0.358139345
N	1532	47.2875	0.29109159
O	1873	49.2635	0.307689398
P	2554	53.0872	0.341225788
Q	3405	47.3931	0.29196649

From Table 1, it is apparent that though samples M, O, and Q follow the expected trend of a higher volume fraction of samples with a lower molecular weight of PHMA, the other samples do not follow this trend. It is this author's belief that the closeness of these samples in the targeted molecular weights of PHMA that some of these samples in actuality could be nearly the same in molecular weight of PHMA. To test this hypothesis, the silica center of each sample will need to be etched with HF and run through a GPC under the appropriate conditions. Samples O and Q have been etched with HF and the GPC results from those samples can be found in Appendix B.

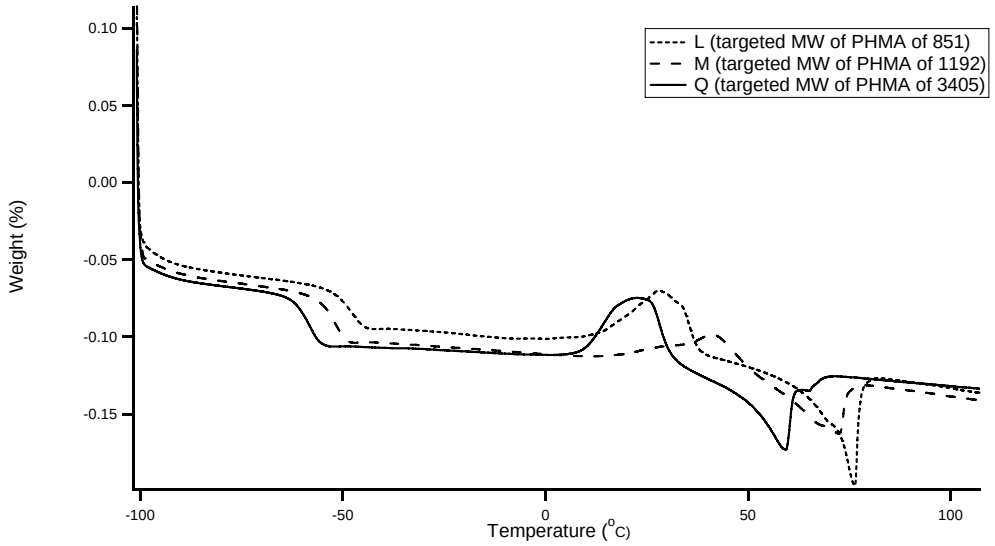

Figure 8. DSC curve for SiO_2-PEG-PHMA samples of varying targeted MW of PHMA. Samples were heated at a rate of 5°C/min from room temperature to 110°C during cycle 1, cooled at a rate of 10°C/min from 110°C to -100°C during cycle 2, and heated at a rate of 5°C/min from -100°C to 110°C during cycle 3. Cycle 3 shown.

Differential scanning calorimetry (DSC) was done using a T. A. Instruments Q1000TA Modulated Differential Scanning Calorimeter under an atmosphere of nitrogen. Samples were heated at a rate of 5°C/min from room temperature to 110°C during cycle 1, cooled at a rate of 10°C/min from 110°C to -100°C during cycle 2, and heated at a rate of 5°C/min from -100°C to 110°C during cycle 3.

Figure 8 shows several important features of the SiO_2-PEG-PHMA samples. First, the presence of only one glass transition temperature around -55°C indicates the presence of a block copolymer. Had this sample been a mixture of PEG and PHMA, two distinct glass transitions would have be seen: one near -5°C for PHMA[39] and one between -80°C and -90°C for PEG[40]. (It should be noted here that according to Huang et al., the glass transition temperature of poly(ethylene glycol) varies greatly with

molecular weight and percentage of absorbed water, thus the broad range for the anticipated T_g of PEG550.[40]) Second, the results show a peak near 25°C that may be contributed to the melting of the polymer. Third, these results clearly show a minimum around 60°C. This minimum is due to crystallization of the polymer.

Dynamic Light Scattering (DLS)

DLS measurements were done on Malvern Instruments Zetasizer Nano. Each sample was suspended in chloroform and filtered through a 0.45 um PTFE filter into a glass cuvette. Figures 9 and 10 show intensity v. size and volume v. size respectively.

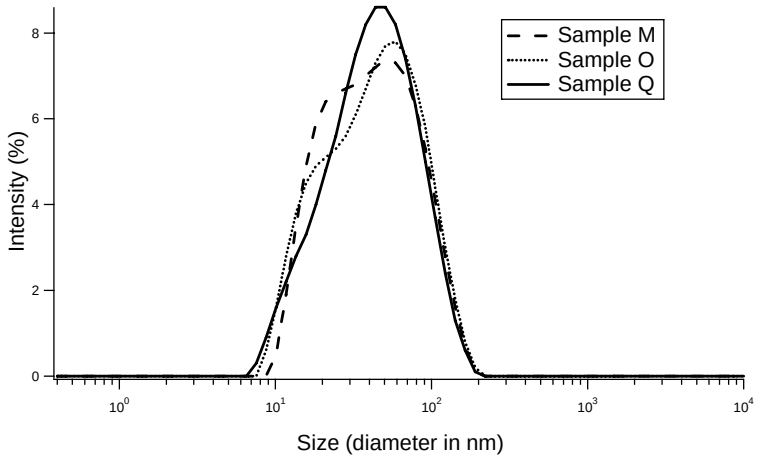

Figure 9. DLS spectrum of Intensity v. Size for SiO_2-PEG-PHMA (samples M, O, and Q).

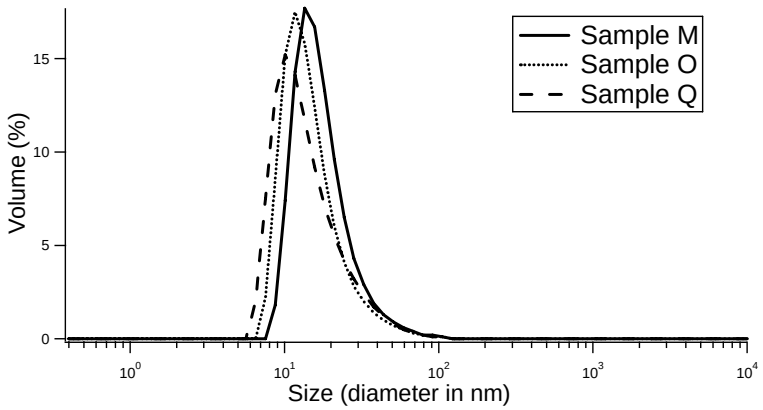

Figure 10. DLS spectrum of Volume v. Size for SiO_2-PEG-PHMA (samples M, O, and Q).

It is instructive to consider both of the graphs when attempting to characterize the particles in each sample. The graph of intensity v. size is more sensitive to larger particles because intensity goes as diameter to the sixth power. As a result, a large particle or aggregation of smaller particles will greatly affect the intensity plot, despite being present in a much lower quantity than the smaller nanoparticles. This sensitivity is both an advantage and a disadvantage. The volume plot is much less sensitive than the intensity plot and gives a more accurate understanding of the diameter of the particle in the system that occupies the most volume in the system.

Table 2. DLS measurements in terms of intensity (%) with resulting averaged size (diameter in nm) for SiO2-PEG-PHMA (samples L, M, N, O, P, Q).

Sample	Z-Ave	Pk 1 Mean	Pk 2 Mean	Pk 1 Area	Pk 2 Area
Name		Intensity	Intensity	Intensity	Intensity
	diameter in nm	diameter in nm	diameter in nm	%	%
L	28.39	54.5	0	100	0
M	34.04	49.35	0	100	0
N	32.07	47.72	0	100	0
O	34.13	51.13	0	100	0
P	34.1	58.72	6.277	97.7	2.3
Q	34.48	49.44	0	100	0

Table 2 shows the data for the intensity v. size plot for each of the six samples in this study. Important in Table 2 is that only sample P shows two peaks in these DLS measurements. Thus sample P is not as pure of a sample as the others and data from this sample should be weighed accordingly.

FT-IR

FT-IR experiments were done using a ThermoScientific Nicolet iZ10 Smart ITR. A background sample was measured before each sample. A total of 64 scans were run per sample.

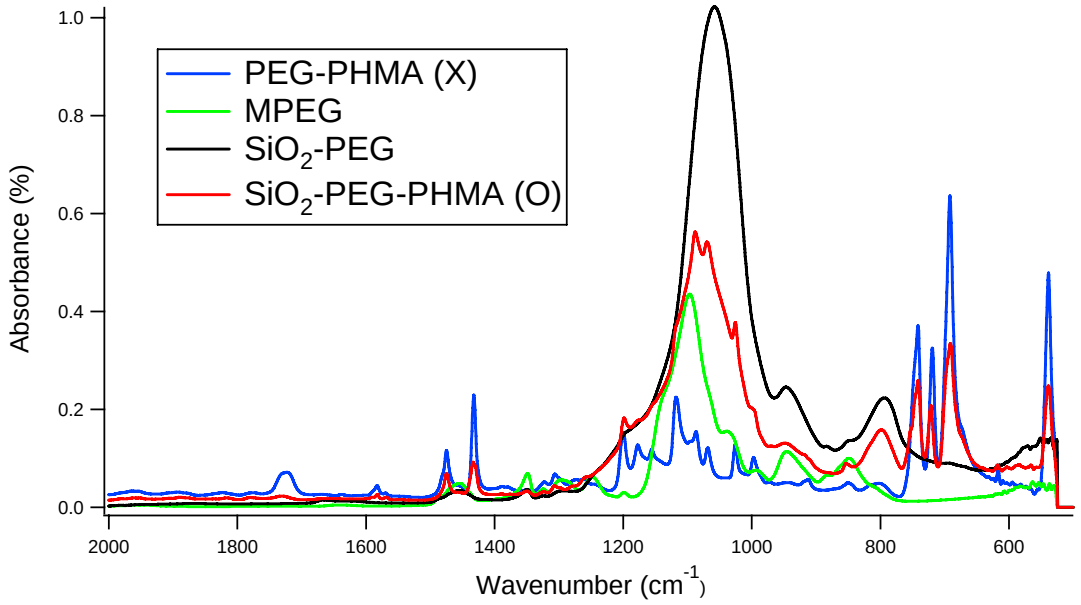

Figure 11. FT-IR spectrum of Absorbance v. Wavenumber for SiO2, MPEG, PHMA, SiO2-PEG-PHMA (sample O).

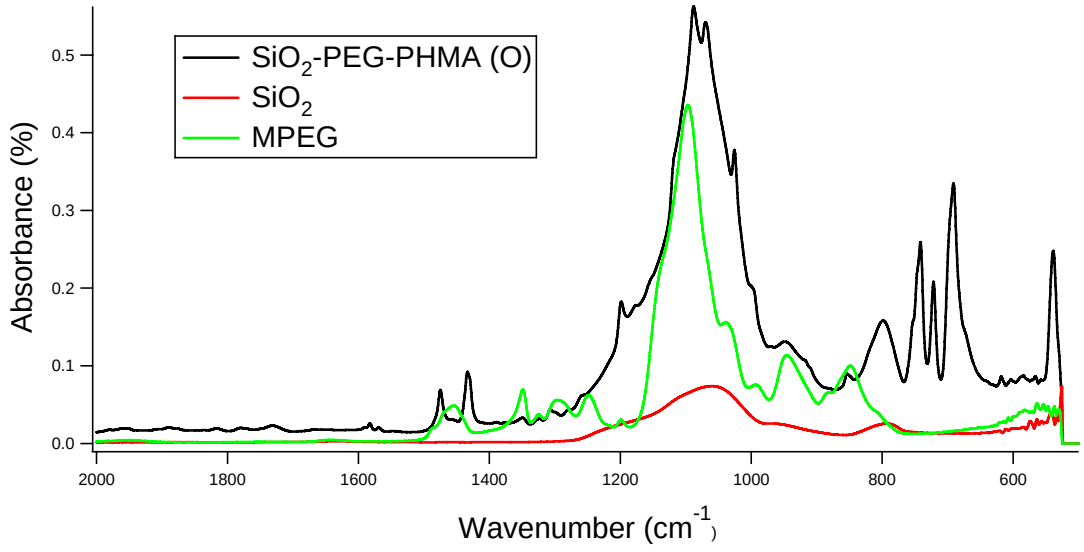

Figure 12. FT-IR spectrum of Absorbance v. Wavenumber for SiO2, MPEG, SiO2-PEG-PHMA (sample O).

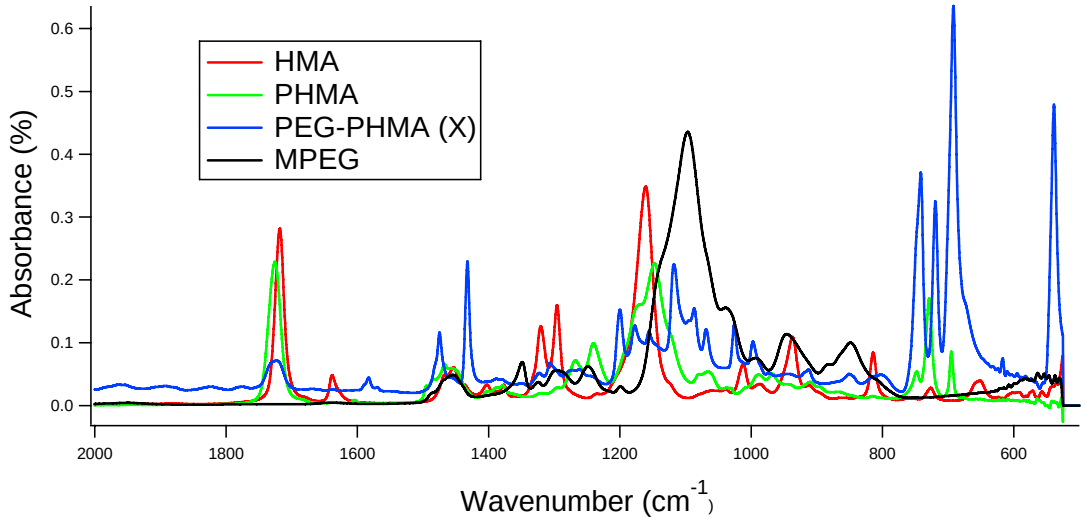

Figure 13. FT-IR spectrum of Absorbance v. Wavenumber for hexyl methacrylate (HMA), PHMA, MPEG, and PEG-PHMA (sample X).

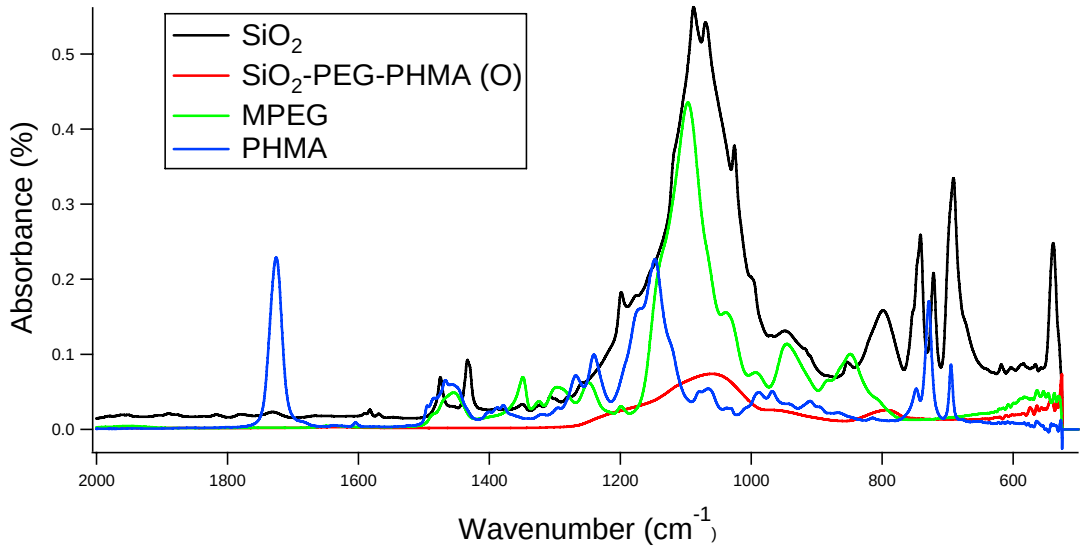

Figure 14. FT-IR spectrum of Absorbance v. Wavenumber for SiO_2-PEG-PHMA (sample O), MPEG, PHMA, and SiO_2.

Figure 11 provides an overall picture of the nature of the SiO2-PEG-PHMA samples.

This spectrum shows that sample O contains SiO2 from the peaks between 1150 cm and 1000 cm and around 800 cm, PEG from the peaks around 1150 ppm and 950 ppm, and 850 ppm, and PHMA from the peaks between 800 and 600. Figures 12-14 show comparisons between sample O and PEG-PHMA, as well as with commercially purchased MPEG, SiO_2, and PHMA.

GPC

GPC experiments were done using a Waters Ambient Temperature GPC with a Waters 486 UV detector and a Waters 2410 differential refractive index detector, operating at 40 ^{o}C with tetrahydrofuran as the eluent. Samples were made 24 hours prior to characterization to a concentration of 1mg/ml and allowed to equilibrate on a mechanical shaker.

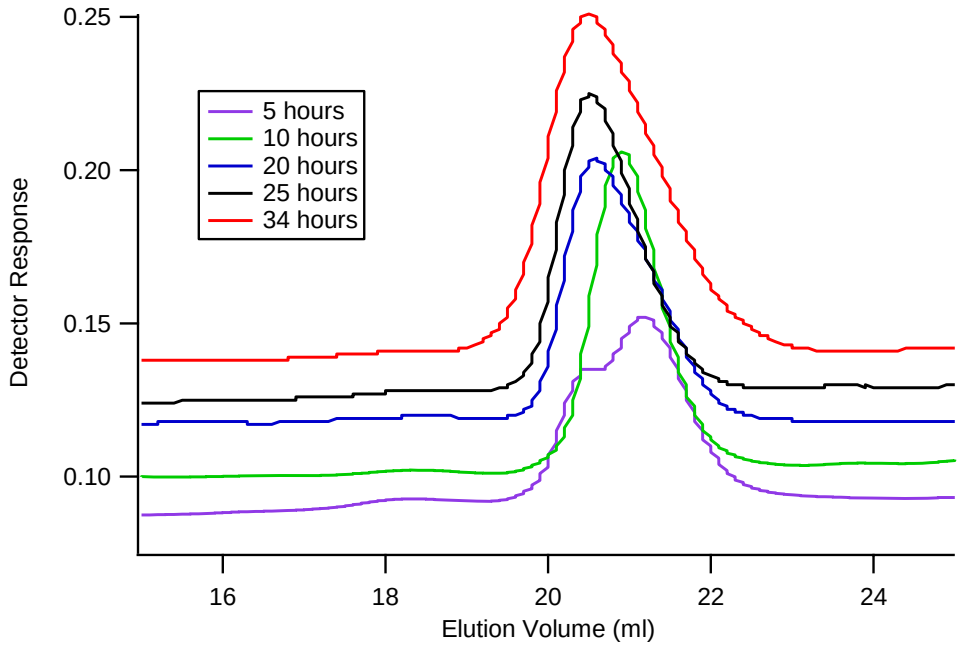

Figure 15. Overlayed GPC elugrams of MPEG-2bb-PHMA aliquots taken at 5, 10, 20, 25, and 34 hours (from PS calibration).

An analysis of the GPC elugrams pertaining to the kinetics study of the MPEG-2bb-PHMA demonstrates that complete conversion is achieved after 10 hours. The ATRP technique yields a bimodal distribution for moderate conversions of PHMA as evidenced by the overlapping peaks seen between 16 and 23 ml of elution volume of the 5 hour sample. However, as the reaction is allowed to progress, the polymer blend becomes less polydisperse as the PHMA conversion increases. Figure 15 reveals a narrowing of the polymer distribution from a polydispersity of 1.605 at 5 hours to 1.222 for the 25 hour sample. The elugrams indicate that the ATRP synthesis follows a living polymerization scheme, and the initial bimodal distribution can be attributed to the polydisperse nature of the MPEG as no effort was made to rigorously separate the MPEG reagent.

Rheology

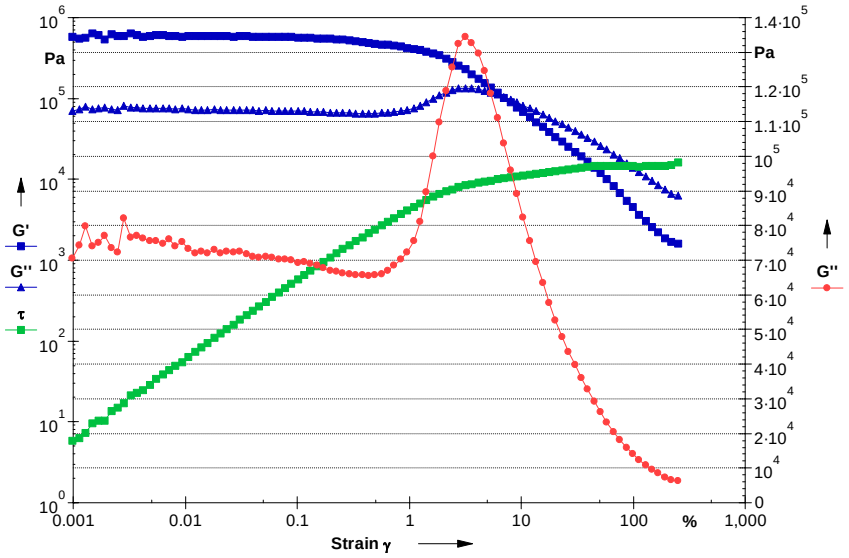

Figure 16. Typical Storage Modulus, Loss Modulus and Shear Stress v. strain curves for SiO_2-PEG-PHMA. Sample O shown with targeted MW of PHMA of 1873. Temperature at 80°C.

Rheology experiments were done using an Anton Parr Physica MCR 300 rheometer with an electrically controlled oven. Depending on the sample, the fixtures used were either a cone and plate fixture of diameter 6 mm or a cone and plate fixture of diameter 10mm. Prior to running the experiments, the gap was zeroed at each temperature, followed by sample loading, a 30 min rest, a preshear to erase thermal history, and a 2 hour rest.

Figure 16 shows typical storage modulus, loss modulus and shear stress v. strain curves for SiO_2-PEG-PHMA. In this figure, the loss modulus (G'') is plotted on both a log scale and a linear scale to emphasize the peak. This peak indicates a yield stress which can be explained using mode-coupling theory.[4] Mode-coupling theory explains

that a maximum in the loss modulus for spherical molecules is due to the confining of each molecule in a cage.[4] The cage must break for the molecule to be released from the cage and flow freely. Each sample shows a yield stress at a certain strain.

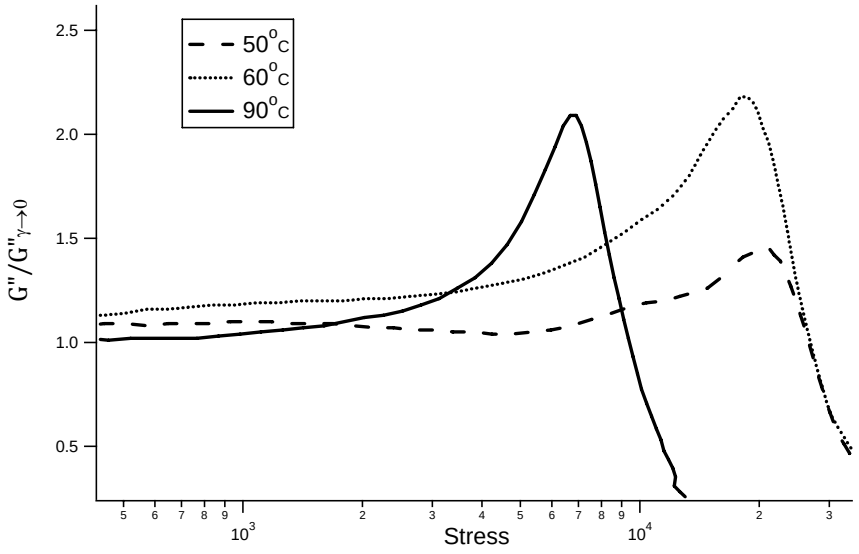

Figure 17. Loss Modulus referenced to the Loss Modulus as the strain approaches zero v. Shear Stress for SiO_2-PEG-PHMA of targeted MW of PHMA of 1873 (sample O) at 50°C, 60°C, and 90°C.

Time-Strain Superposition

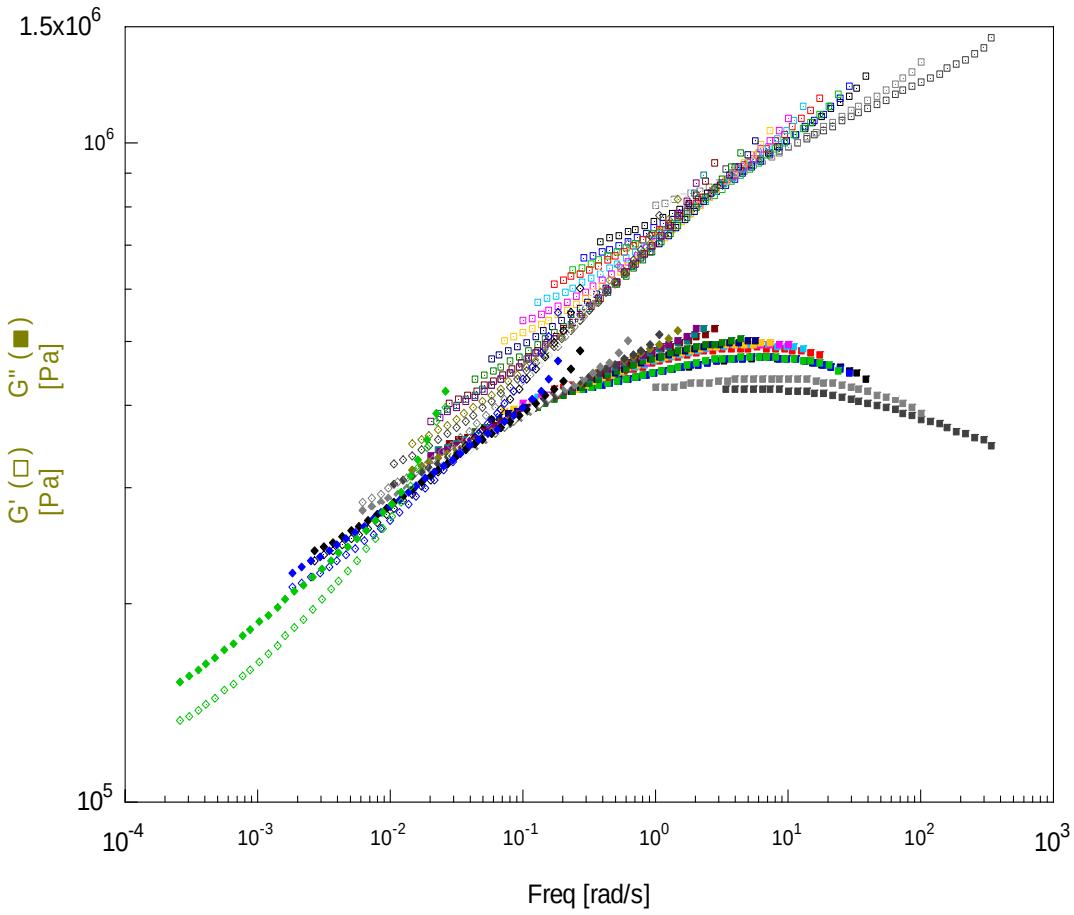

Figure 18. Time-Strain Superposition master curve for SiO2-PEG-PHMA (sample Q) at 90^{o} C. The reference strain is 2.04543.

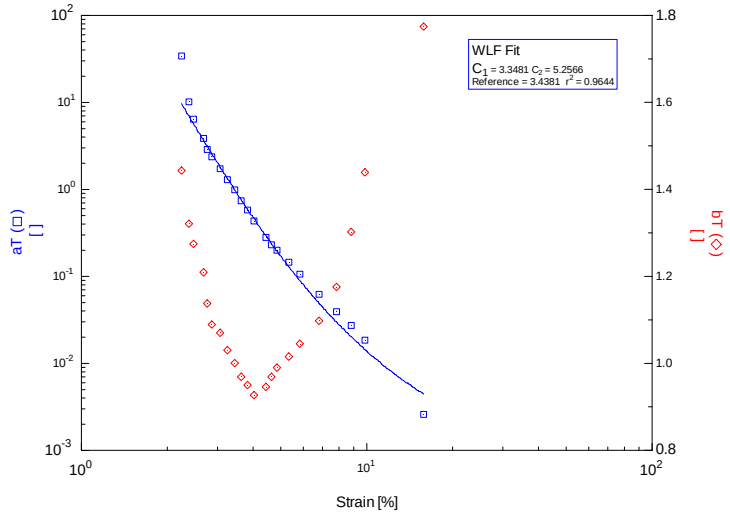

Figure 19. Fitting Parameters for Time-Strain Superposition master curve shown in Figure 18. Plot includes WLF fit equation with r^2 value of 0.9644 with respect to bT. The shift factor aT corresponds to the horizontal shift in the data and bT corresponds to the vertical shift in the data.

The benefit of obtaining a master curve from time-strain superposition is that it allows one to obtain dynamic data over frequencies not easily accessible on normal instrumentation.[41] Typically, this master curve is achieved using temperature data and is termed time-temperature superposition. The WLF equation with respect to time-temperature superposition and time-strain superposition is essentially the same. The only difference is using various strains in the equation instead of temperatures.[4] Figure 18 is one such curve for sample Q. This figure shows a broad maximum in the loss modulus near a frequency of 1 rad/s. This author recommends further studies in this area to determine if all of the samples show similar maxima in their master curves, or if this is unique to this particular sample. The time-temperature superposition curve for this sample shows better overlay at higher frequencies though deviation is still

apparent. More research will need to be done to determine if these deviations are due to contamination in the sample perhaps from trace amounts of residual catalyst causing slight alterations to the results owing to the high sensitivity of the instrument, to poor selection of frequencies to be scanned owing to the small body of knowledge available for these compounds, or to the NOHMS themselves and perhaps inherent fluctuations in the storage and loss moduli at various frequencies due to the inorganic/organic interactions.

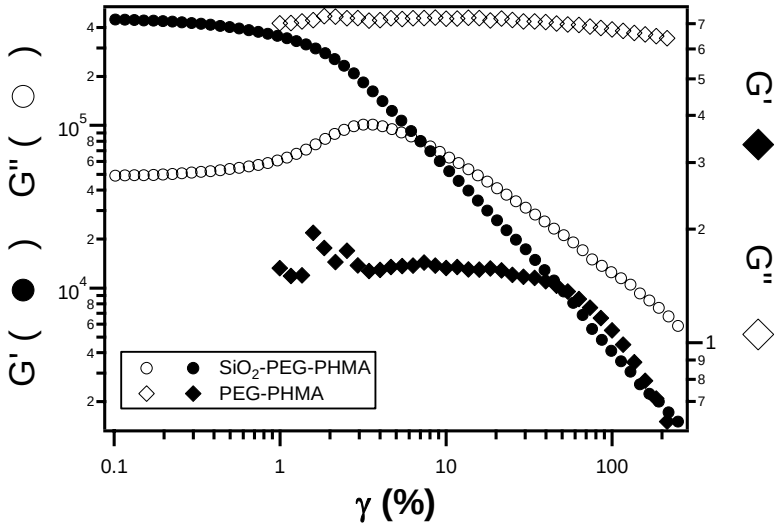

Figure 20. Comparison of the Storage Modulus (G') and the Loss Modulus (G") for SiO_2-PEG-PHMA (sample O) and PEG-PHMA (sample Y).

Figure 20 compares the storage modulus (G') and the loss modulus (G") for two samples with similar targeted molecular weights of PHMA, SiO_2-PEG-PHMA (sample O) and PEG-PHMA (sample Y). It is interesting to note here the difference in magnitude between G' and G" between the two samples as well as the presence of a maximum in G" in the SiO_2-PEG-PHMA sample but not in the PEG-PHMA sample. These clear differences between two samples due to the inclusion of nanoparticles illustrate the need to better understand the nanoparticle-polymer interactions.

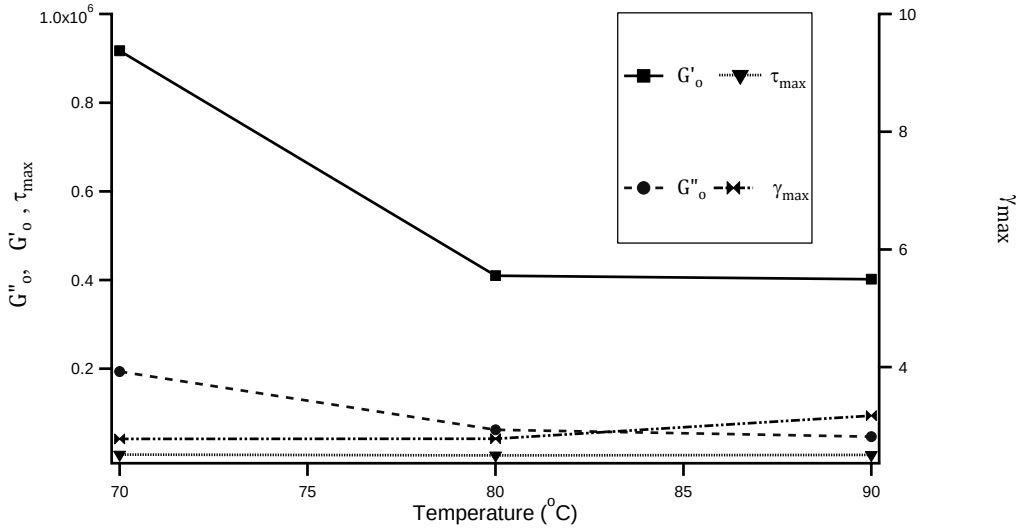

Figure 21. Comparison of the Storage Modulus (G_0') and Loss Modulus (G_0'') as the strain tends toward zero and the strain (γ_{max}) and stress (τ_{max}) at the maximum in the Loss Modulus for SiO_2-PEG-PHMA (sample O) at 90 °C.

Figure 21 compares the storage modulus (G_0') and loss modulus (G_0'') as the strain tends toward zero and the strain (γ_{max}) and stress (τ_{max}) at the maximum in the loss modulus for SiO_2-PEG-PHMA (sample O). Though not extensive or conclusive, this plot begins to show a decreasing trend in G_0' and G_0'' as temperature increases. This trend is important to understand should these NOHMS be used in industry and certainly requires a more exhaustive study.

CONCLUSIONS AND RECOMMENDATIONS

Novel nanoparticle-organic hybrid molecules have been synthesized with a silica core. A triethoxysilane-PEG of molecular weight between 400 and 550 was used to functionalize 8 nm silica nanoparticles. An ATRP initiator was reacted with the PEG attached to the silica nanoparticles, and then reacted with hexyl methacrylate using atom transfer radical polymerization. TGA confirms the presence of inorganic material. DSC confirms the presence of a block copolymer. DLS confirms the presence of a low polydisperse hybrid material. The rheological properties of this material were studied. The material is shown to have a G_0' and G_0'' that depend upon temperature, though more study is needed in this area.

APPENDIX A

Removal of the copper catalyst in the ATRP of styrene

Removal of this catalyst was important for several reasons. In terms of the viablility of industrial production, the presence of a catalyst has the potential to discolor, make toxic, and weaken the mechanical properties of the final product.[42]

In these experiments, removal of the catalyst was a non-trivial problem and there are several suggested solutions found in the literature.[43-50] Haddleton et al. used surface-immobilized catalysts but this resulted in polymers with broader molecular weight distributions.[51] Honigfort et al. used precipitons attached to nitrogen ligands coordinated with a copper center.[45] Precipitons are soluble in organic solvents when in the *cis*-form, but insoluble in the *trans*-form.[45] This insolubility allowed Honingfort et al. to easily remove the ligands complexed with the copper catalyst via centrifugation after exposure to UV light.[45] The concern here is that the method to produce the precipitons is financialy costly, time intensive, and the catalyst is not recyclable. Matyjaszewski et al. reduced the amount of copper catalyst needed to between 10 and 50 ppm by using a constant source of organic free radicals to regenerate the copper catalyst[44]. Matyjaszewski et al. term this method "initiators for continuous activator regeneration, ICAR."[44] Much research into this method is needed to determine the appropriate source of free radicals, the amount of copper catalyst needed with the source of free radicals, the appropriate ligand, as well as the monomer and solvent system.[44, 49] Since this background research was not the focus of this study, this author chose not to use this method. Faucher et al. precipitated their chosen catalyst system of $Cu^{I}Br$/nitrogen ligand through addition of $Cu^{II}Br_2$.[47] This precipitate was then filtered using a 0.1 μm PTFE filter.[47] ICP analysis revealed the

copper concentration dropped from 200-400 ppm to 10-50 ppm.[47] This method is therefore useful, but only for small scale purification.

This author considered three approaches for catalyst removal, ion-exchange resins[48], extraction using ethylenediaminetetraacetic acid (EDTA)[46], and passage through a column of neutral alumina.[43, 52] Of these methods, the fastest, easiest and most thorough was removal using a column of neutral alumina. Since this column removal had been proven successful, when the focus of the project changed from styrene with a copper catalyst to hexyl methacrylate with a nickel catalyst, the author chose to use a column of alumina, as used by Mahajan et. al.[5]

APPENDIX B

Table 3. Molecular Weight In polystyrene Equivalents and Polydispersity Index (PDI) for SiO_2-PEG-PHMA, samples O and Q, after HF etching.

Sample	Targeted MW of PHMA	Targeted MW of PHMA and PEG	MW in polystyrene equivalents after HF etch	PDI from GPC
O	1873	2423	44869	1.35
Q	3405	3955	1476.1	1.002

Table 3 and Figures 22-25 show the GPC results from samples O and Q after HF etching. The results for sample O seem reasonable, but for sample Q, it is this author's belief that one of three reasons for the small peak are possible. First, the samples may not have been as soluble in THF as the GPC requires (this is supported by the very large residue peak at the beginning of sample Q, possibly residue from sample O, as these samples were run back to back.) Second, the sample may have been too large to be detected by the columns on the GPC. This is also supported by the large peak at the beginning of the sample. A reason for the large sample molecular weight could be that though the etching worked for the silica nanoparticles, maybe the triethoxysilane groups at the end of the silane-PEG cross-linked and thus the result from the HF etching was a hollow polymer shell held together by these silane cross-links. Lastly, perhaps sample Q was not of high enough concentration for detection. Regardless of the reason, these samples should be etched and run again through the GPC.

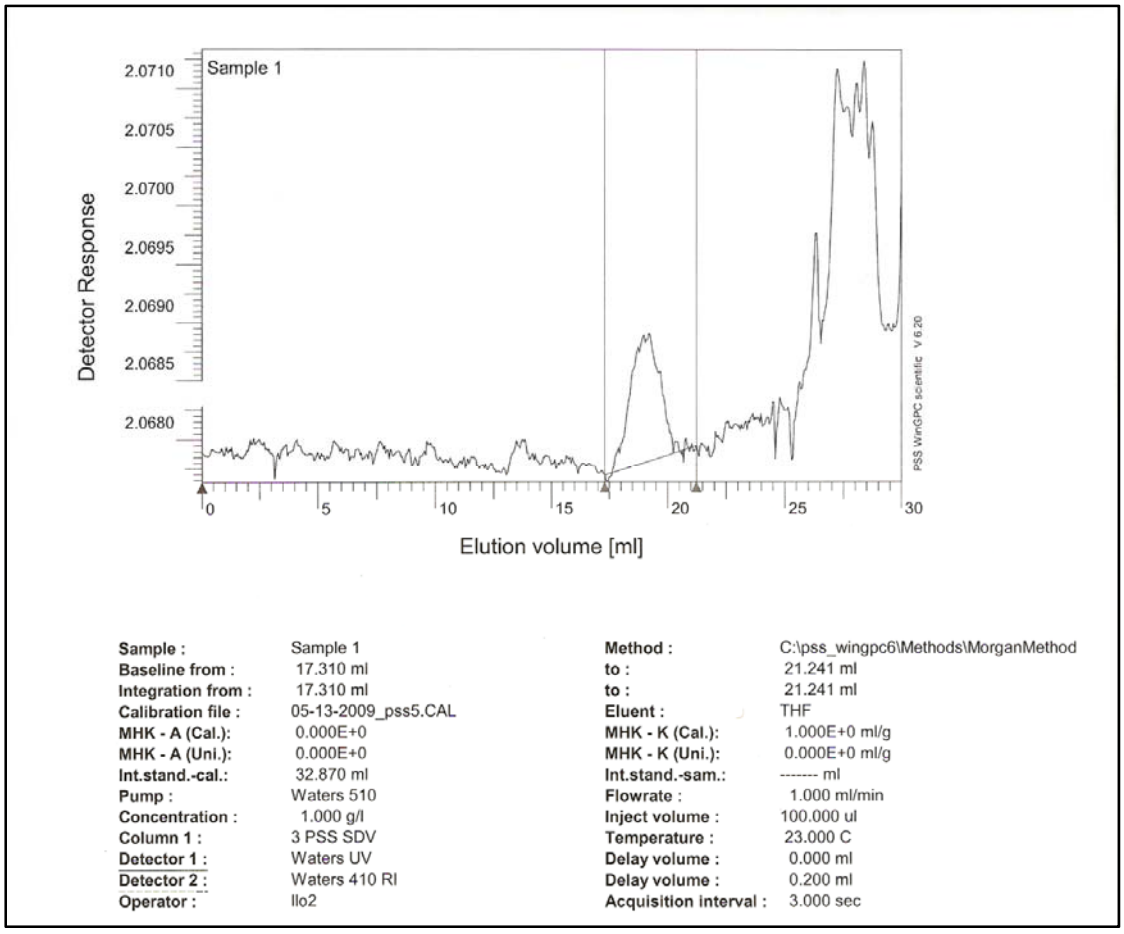

Figure 22. GPC elugram and corresponding data for SiO_2-PEG-PHMA (sample O) after HF etching. Peak shown selected here (between the two vertical lines) is amplified in Figure 23.

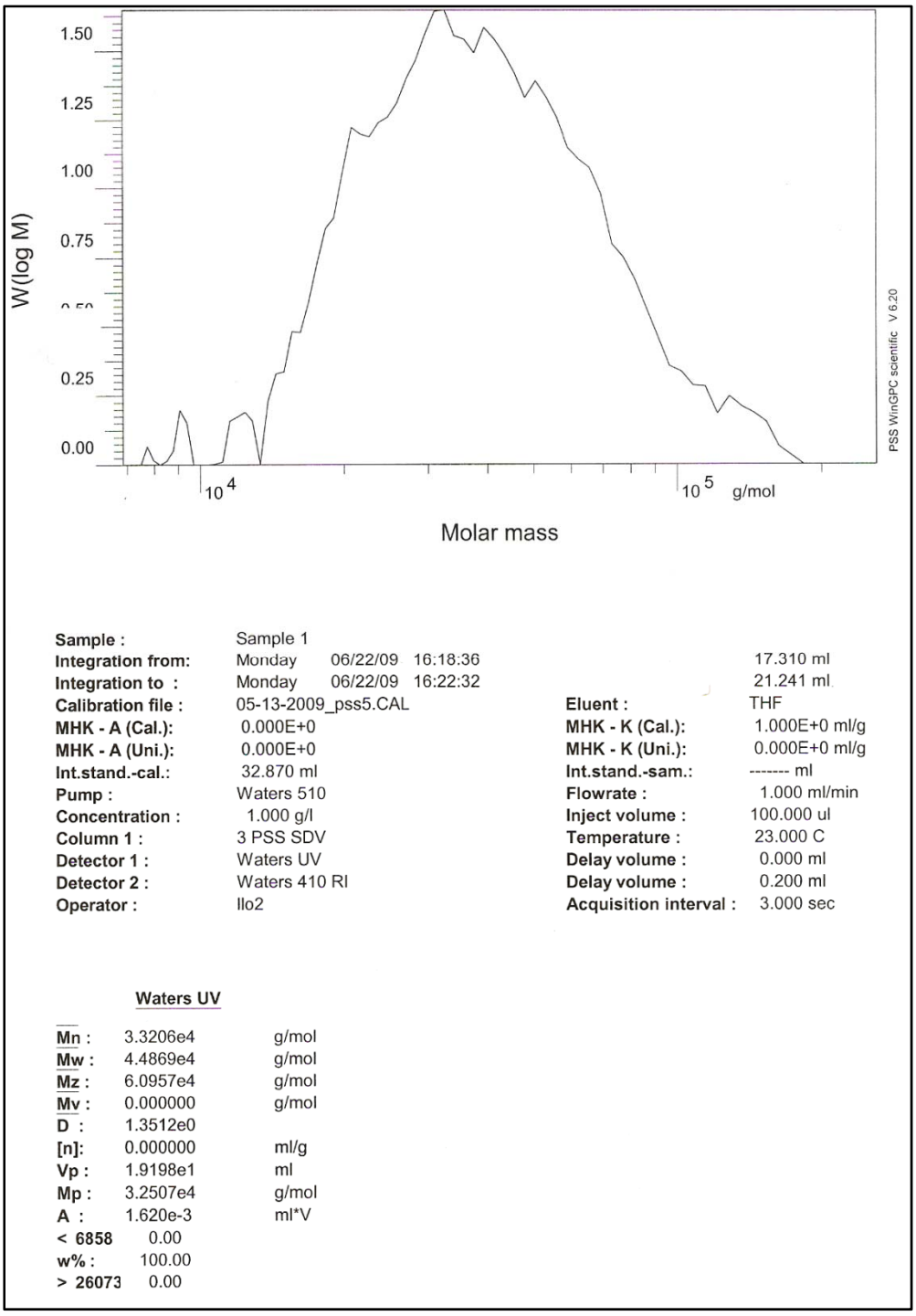

Figure 23. GPC data from the selected peak in Figure 22 for SiO_2-PEG-PHMA (sample O).

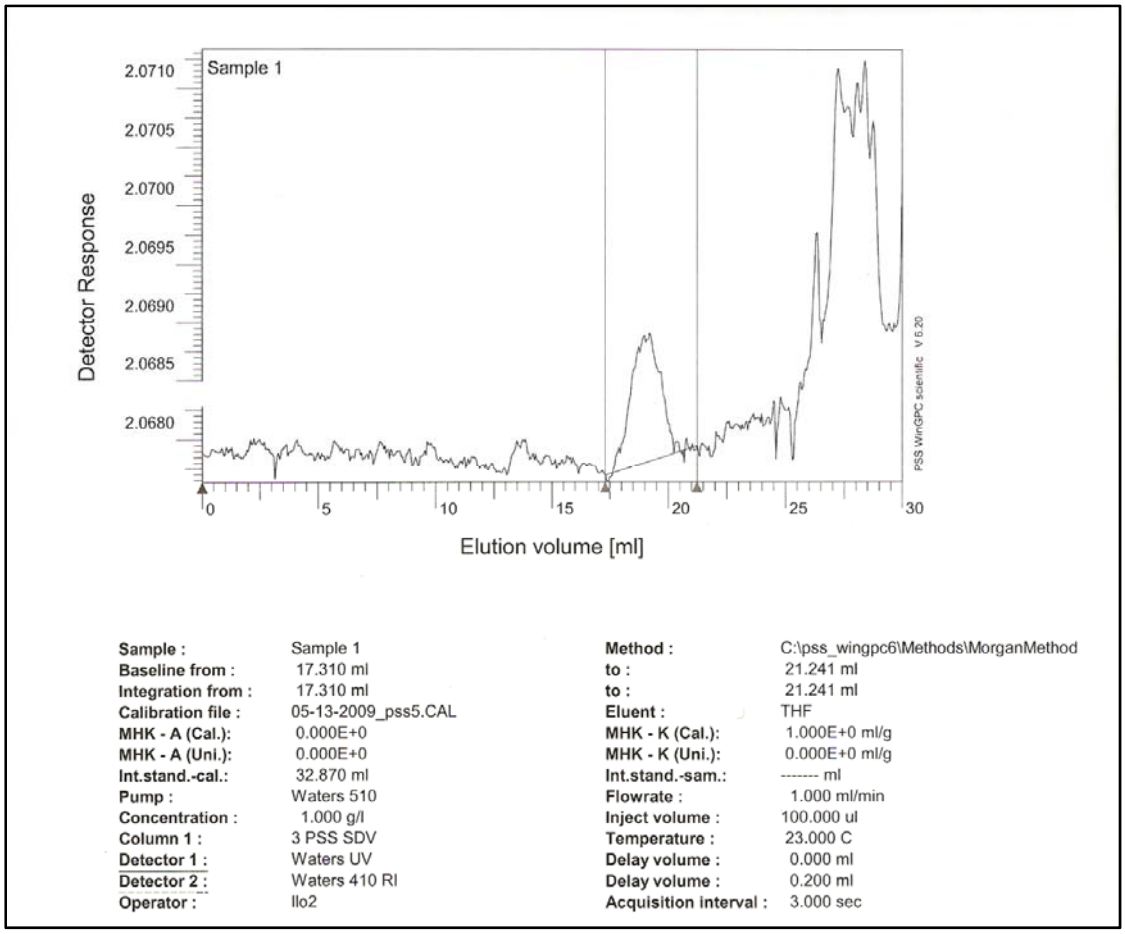

Figure 24. GPC elugram and corresponding data for SiO_2-PEG-PHMA (sample Q) after HF etching. Peak shown selected here (between the two vertical lines) is amplified in Figure 25.

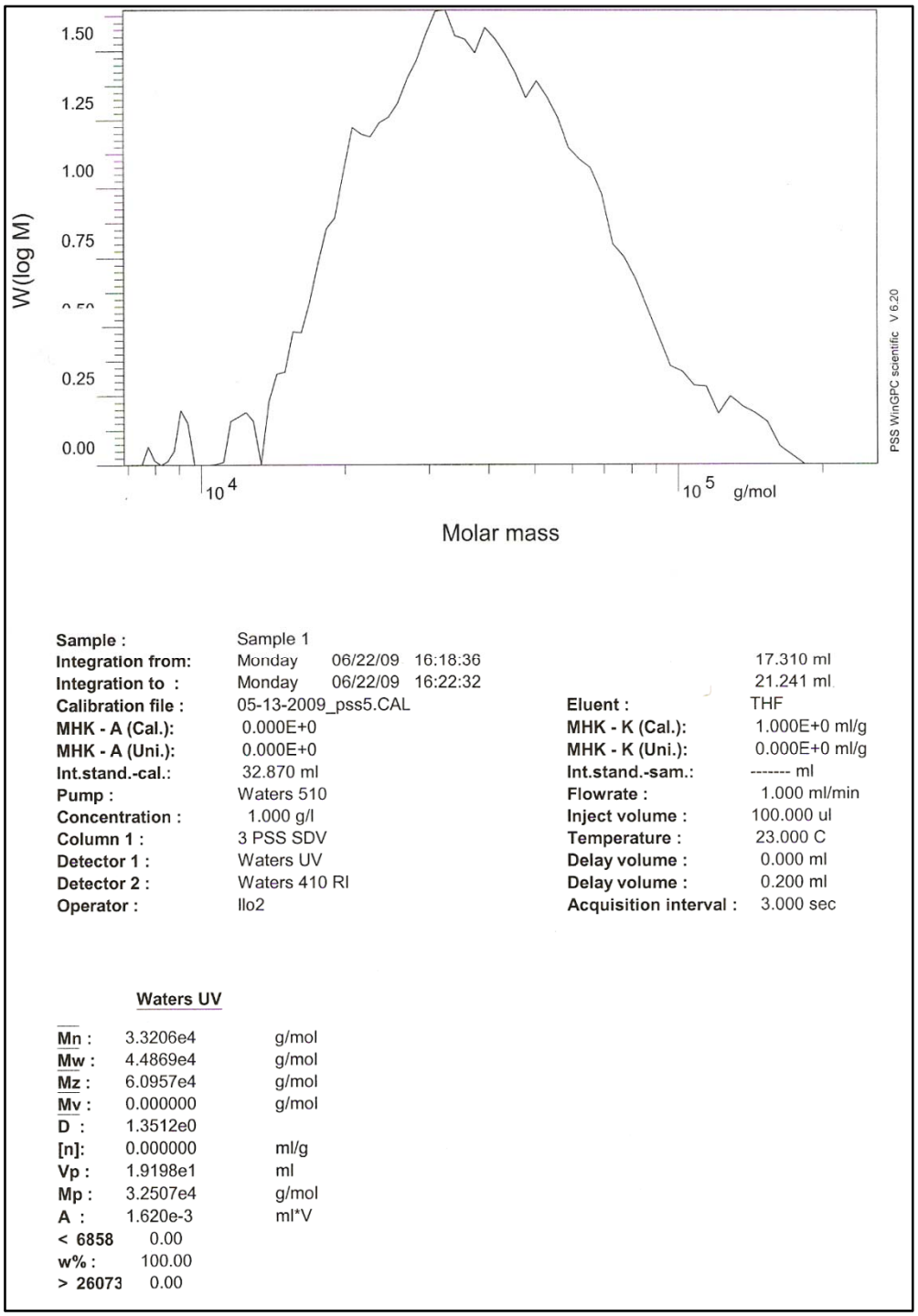

Sample :	Sample 1		
Integration from:	Monday 06/22/09 16:18:36		17.310 ml
Integration to :	Monday 06/22/09 16:22:32		21.241 ml
Calibration file :	05-13-2009_pss5.CAL	**Eluent :**	THF
MHK - A (Cal.):	0.000E+0	**MHK - K (Cal.):**	1.000E+0 ml/g
MHK - A (Uni.):	0.000E+0	**MHK - K (Uni.):**	0.000E+0 ml/g
Int.stand.-cal.:	32.870 ml	**Int.stand.-sam.:**	------- ml
Pump :	Waters 510	**Flowrate :**	1.000 ml/min
Concentration :	1.000 g/l	**Inject volume :**	100.000 ul
Column 1 :	3 PSS SDV	**Temperature :**	23.000 C
Detector 1 :	Waters UV	**Delay volume :**	0.000 ml
Detector 2 :	Waters 410 RI	**Delay volume :**	0.200 ml
Operator :	Ilo2	**Acquisition interval :**	3.000 sec

Waters UV

Mn :	3.3206e4	g/mol
Mw :	4.4869e4	g/mol
Mz :	6.0957e4	g/mol
Mv :	0.000000	g/mol
D :	1.3512e0	
[n]:	0.000000	ml/g
Vp :	1.9198e1	ml
Mp :	3.2507e4	g/mol
A :	1.620e-3	ml*V
< 6858	0.00	
w% :	100.00	
> 26073	0.00	

Figure 25. GPC data from the selected peak in Figure 24 for SiO_2-PEG-PHMA (sample Q).

REFERENCES

1. Matyjaszewski, K.; Xia, J., Atom Tranfer Radical Polymerization. *Chemical Reviews* **2001,** 101, 2921-2990.

2. Zou, H.; Wu, S.; Shen, J., Polymer/Silica Nanocomposites: Preparation, Characterization, Properties, and Applications. *Chemical Reviews* **2008,** 108, (9), 3893-3957.

3. El Harrak, A.; Carrot, G.; Oberdisse, J.; Jestin, J.; Boue, F., Atom transfer radical polymerization from silica nanoparticles using the 'grafting from' method and structural study via small-angle neutron scattering. *Polymer* **2005,** 46, 1095-1104.

4. Larson, R. G., *The Structure and Rheology of Complex Fluids*. Oxford University Press: New York, 1999.

5. Mahajan, S.; Renker, S.; Simon, P. F. W.; Gutmann, J.; Jain, A.; Gruner, S. M.; Fetters, L. J.; Coates, G. W.; Wiesner, U., Synthesis and Characterization of Amphiphilic Poly(ethylene oxide)-block-poly(hexyl methacrylate) Copolymers. *Macromolecular Chemistry and Physics* **2003,** 2003, (204), 1047-1055.

6. Mahajan, S.; Cho, B.-K.; Allgaier, J.; Fetters, L. J.; Coates, G. W.; Wiesner, U., Synthesis of Amphiphilic ABC Triblock Copolymers with PEO as the Middle Block. *Macromolecular Rapid Communications* **2004,** 25, 1889-1894.

7. Ramanathan, N.; Hatton, T. A., Eds., *Nanoparticles: Synthesis, Stabilization, Passivation and Functionalization*. American Chemical Society: Washington, DC, 2008.

8. Bauer, F.; Ernst, H.; Decker, U.; Findeisen, M.; Glasel, H.-J.; Langguth, H.; Hartmass, E.; Mehnert, R.; Peuker, C., Preparation of scratch and abrasion resistant polymeric nanocomposites by monomer grafting onto nanoparticles, FTIR and multi-nuclear NMR spectroscopy to the characterization of methacryl grafting. *Macromolecular Chemistry and Physics* **2000,** 201, 2654-2659.

9. Jang, J.; Ha, J.; Kim, B., Synthesis and characterization of monodisperse silica-polyaniline core-shell nanoparticles. *Chemical Communications* **2006**, 1622-1624.

10. Sondi, I.; Fedynyshyn, T. H.; Sinta, R.; Matijevi, E., Encapsulation of Nanosized Sillica by in Situ Polymerization of tert-Butyl Acrylate Monomer. *Langmuir* **2000,** 16, (23), 9031-9034.

11. Rodriguez, J. A.; Fernandez-Garcia, M., *Synthesis, Properties, and Applications of Oxide Nanoparticles*. John Wiley & Sons, Inc.: Hoboken, NJ, 2007.

12. Nagarajan, R., *Nanoparticles: Synthesis, Stabilization, Passivation and Functionalization*. 2008; Vol. Chapter 1, pp 2-14.

13. Kali, G.; Georgiou, T. K.; Ivan, B.; Patrickios, C. S.; Loizou, E.; Thomann, Y.; Tiller, J., *Nanoparticles: Synthesis, Stabilization, Passivation and Functionalization*. American Chemical Society: Washington, DC, 2008; p Chapter 21, pp 286-302.

14. Zhang, K.; Li, H.; Zhao, S.; Wang, W.; Wang, S.; Xu, Y., Synthesis and characterization of polymer brushes containing metal nanoparticles. *Polymer Bulletin* **2006,** 57, 253-259.

15. Chen, Y.; Kang, E.-T.; Neoh, K.-G.; Greiner, A., Preparation of Hollow Sillica Nanospheres by Surface-Initiated Atom Transfer Radical Polymerization on Polymer Latex Templates. *Advanced Functional Materials* **2005,** 15, (1), 113-117.

16. Savin, D. A.; Pyun, J.; Patterson, G. D.; Kowalewski, T.; Matyjaszewski, K., Synthesis and Characterization of Silica-*graft*-Polystyrene Hybrid Nanoparticles: Effect of Constraint on the Glass-Transition Temperature of Spherical Polymer Brushes. *Journal of Polymer Science: Part B: Polymer Physics* **2002,** 40, 2667-2676.

17. Etienne, S.; Becker, C.; Ruch, D.; Grignard, B.; Cartigny, G.; Detrembleur, C.; Calberg, C.; Jerome, R., Effects of Incorporation of Modified Silica Nanoparticles on the Mechanical and Thermal Properties of PMMA. *Journal or Thermal Analysis and Calorimetry* **2007,** 87, (1), 101-104.

18. Kamigaito, M.; Ando, T.; Sawamoto, M., Metal-Catalyzed Living Radical Polymerization. *Chemical Reviews* **2001,** 101, 3689-3745.

19. Korth, B. D.; Keng, P. Y. S., Inbo; Tang, C.; Pyun, J., *Nanoparticles: Synthesis, Stabilization, Passivation and Functionalization*. American Chemical Society: Washington, DC, 2008; p Chapter 20, pp 272-285.

20. El Harrak, A.; Carrot, G.; Oberdisse, J.; Jestin, J.; Boue, F., Control of the Colloidal Stability of Polymer-Grafted-Silica Nanoparticles Obtained by Atom Transfer Radical Polymerization. *Macromolecular Symposium* **2005,** 226, 263-278.

21. Coessens, V.; Pintauer, T.; Matyjaszewski, K., Functional Polymers by Atom Transfer Radical Polymerization. *Progress in Polymer Science* **2001,** 26, 337-377.

22. Zhou, L.; Yuan, W.; Yuan, J.; Hong, X., Preparation of double-responsive SiO_2-g-PDMAEMA nanoparticles *via* ATRP. *Materials Letters* **2008,** 62, 1372-1375.

23. Patten, T. E.; Xia, J.; Abernathy, T.; Matyjaszewski, K., Polymers with Very Low Polydispersities from Atom Transfer Radical Polymerization. *Science* **1996,** 272, 866-868.

24. Ramakrishnan, A.; Dhamodharan, R., Facile Synthesis of ABC and CBABC Multiblock Copolymers of Styrene, *tert*-Butyl Acrylate and Methyl Methacrylate via Room Temperature ATRP of MMA. *Macromolecules* **2003,** 36, 1039-1046.

25. Patten, T. E.; Matyjaszewski, K., Atom Transfer Radical Polymerization and the Synthesis of Polymeric Materials. *Advanced Materials* **1998,** 10, (12), 901-915.

26. Odian, G., *Principles of Polymerization*. Fourth ed.; John Wiley & Sons, Inc.: Hoboken, NJ, 2004.

27. Matyjaszewski, K.; Davis, T. P., *Handbook of Radical Polymerization*. John Wiley & Sons, Inc.: Hoboken, 2002.

28. Johnson, R. M.; Ng, C.; Samson, C. C. M.; Fraser, C. L., Copper ATRP Catalysts with Quadridentate Amine Ligands: The Effects of Steric and Electronic Tuning on the Polymerization of Methyl Methacrylate. *Macromolecules* **2000,** 33, (23), 8618-8628.

29. Qui, J.; Matyjaszewski, K.; Thouin, L.; Amatore, C., Cyclic voltammetric studies of copper complexes catalyzing atom transfer radical polymerization. *Macromolecular Chemistry and Physics* **2001,** 210, 1625-1631.

30. Ando, T.; Kamigaito, M.; Sawamoto, M., Catalytic Activities of Ruthenium(II) Complexes in Transition-Metal-Mediated Living Radical Polymerization: Polymerization, Model Reaction, and Cyclic Voltammetry. *Macromolecules* **2000,** 33, 5825-5829.

31. Tsarevsky, N. V.; Braunecker, W. A.; Matyjaszewski, K., Electron transfer reactions relevant to atom transfer radical polymerization. *Journal of Organometallic Chemistry* **2007,** 692, 3212-3222.

32. Tang, W.; Matyjaszewski, K., Effects of Initiator Structure on Activation Rate Constants in ATRP. *Macromolecules* **2007,** 40, 1858-1863.

33. Xu, Y.; Lu, J.; Xu, Q.; Wang, L., Atom transfer radical polymerization of styrene initiated by triphenylmethyl chloride. *European Polymer Journal* **2005,** 41, 2422-2427.

34. Ando, T.; Kamigaito, M.; Sawamoto, M., Metal Alkoxides as Additives for Ruthenium(II)-Catalyzed Living Radical Polymerization. *Macromolecules* **2000,** 33, (18), 6732-6737.

35. Uegaki, H.; Kotani, Y.; Kamigaito, M.; Sawamoto, M., Nickel-Mediated Living Radical Polymerization of Methyl Methacrylate. *Macromolecules* **1997,** 30, (8), 2249-2253.

36. Mandal, T. K.; Fleming, M. S.; Walt, D. R., Production of Hollow Polymeric Microspheres by Surface-Confined Living Radical Polymerization on Silica Templates. *Chemical Materials* **2000,** 12, 3481-3487.

37. Lide, D. R., *CRC Handbook of Chemistry and Physics*. CRC Press I, LLC: Boca Raton, FL, 2008-2009; p 4-88.

38. http://www.scientificpolymer.com/resources/poly_dens_alpha.asp

39. Lide, D. R., *CRC Handbook of Chemistry and Physics*. 89th ed.; CRC Press I, LLC: Boca Raton, FL, 2008-2009; p 13-7.

40. Huang, L.; Nishinari, K., Interaction between poly(ethylene glycol) and water as studied by Differential Scanning Calorimetry. *Journal of Polymer Science: Part B: Polymer Physics* **2001,** 39, 496-506.

41. Gupta, R. K., *Polymer and Composite Rheology*. Second ed.; Marcel Dekker, Inc.: New York, 2000.

42. Goerlitzer, H.; Staschik, D. Method for removing metal ions from polymers or polymer solutions U.S. Patent 20050199549, 2005.

43. Brar, A. S.; Puneeta, Synthesis of Styrene/Methyl Methacrylate Copolymers by Atom Transfer Radical Polymerization: 2D NMR Investigations. *Journal of Polymer Science: Part A: Polymer Chemistry* **2006,** 44, 2076-2085.

44. Matyjaszewski, K.; Jakubowski, W.; Min, K.; Tang, W.; Huang, J.; Braunecker, W. A.; Tsvarevsky, N. V., Diminishing catalyst concentration in atom transfer radical polymerization with reducing agents. *Proceedings of the National Academy of Sciences* **2006,** 103, (42), 15309-15314.

45. Honigfort, M. E.; Brittain, W. J., Use of Precipitons for Copper Removal in Atom Transfer Radical Polymerization. *Macromolecules* **2002,** 35, (13), 4849-4851.

46. Shen, Y.; Tang, H.; Ding, S., Catalyst separation in atom transfer radical polymerization. *Progress in Polymer Science* **2004,** 29, (1053-1078).

47. Faucher, S.; Okrutny, P.; Zhu, S., Facile and Effective Purification of Polymers Produced by Atom Transfer Radical POlymerization via Simple Catalyst Precipitation and Microfiltration. *Macromolecules* **2006,** 39, 3-5.

48. Pintauer, T.; Gaynor, S.; Matyjaszewski, K., Removal of Catalyst in Atom Transfer Radical Polymerization using Cross-Linked Polystyrene Ion-Exchange Resins. *Abstracts of Papers of the American Chemical Society* **1999,** 218, 497-POLY.

49. Tsvarevsky, N. V.; Matyjaszewski, K., "Green" Atom Transfer Radical Polymerization: From Process Design to Preparation of Well-Defined Environmentally Friendly Polymeric Materials. *Chemical Reviews* **2007,** 107, 2270-2299.

50. Matyjaszewski, K.; Pintauer, T.; Gaynor, S., Removal of Copper-Based Catalyst in Atom Transfer Radical Polymerization using Ion Exchange Resins. *Macromolecules* **2000,** 33, 1476-1478.

51. Haddleton, D. M.; Duncalf, D. J.; Kukulji, D.; Radigue, A. P., 3-Aminopropyl Silica Supported Living Radical Polymerization of Methyl Methacrylate: Dichlorotris(triphenylphosphine)ruthenium(II) Mediated Atom Transfer Polymerization. *Macromolecules* **1999,** 32, (15), 4769-4775.

52. Wang, T.-L.; Liu, Y.-Z.; Jeng, B.-C.; Cai, Y.-C., The Effect of Initiators and Reaction Conditions on the Polymer Syntheses by Atom Transfer Radical Polymerization. *Journal of Polymer Research* **2005,** 12, 67-75.